

Cite this: DOI: 10.1039/d0ta08107h

## N-Methyl-2-pyrrolidone-promoted crystallization of MEL zeolite and its acceleration mechanism†

Chuanyu Yang,<sup>‡ab</sup> Dongpu Zhao,<sup>‡ab</sup> Weifeng Chu,<sup>a</sup> Yanan Wang,<sup>a</sup> Xiujie Li,<sup>a</sup> Sujuan Xie,<sup>a</sup> Wenjie Xin,<sup>a</sup> Xiangxue Zhu,<sup>✉\*a</sup> Shenglin Liu<sup>\*a</sup> and Longya Xu<sup>✉\*a</sup>

ZSM-11 zeolite is an important microporous material that has wide application prospects in various petrochemical and chemical processes. Herein, we reported a simple method to significantly reduce the crystallization time of ZSM-11 zeolite by adding *N*-methyl-2-pyrrolidone (NMP) as the 'promoter'. The effects of various synthetic parameters on the NMP-assisted synthesis of ZSM-11 zeolite were also investigated. Subsequently, characterization techniques such as SEM, XRD, XRF, FT-IR, TEM-EDS, TG and <sup>13</sup>C NMR were used to unveil the acceleration mechanism of NMP. It was revealed that NMP can facilitate the bonding of TBA<sup>+</sup> with aluminosilicate by breaking the hydration layer around them, thus reducing the apparent nucleation activation energy and accelerating the nucleation process. Meanwhile, we used *N*-ethyl-2-pyrrolidone (NEP) instead of NMP as the promoter to verify the acceleration mechanism. In addition, the fast-synthesized ZSM-11 zeolite exhibited comparable composition, hydrothermal stability, and catalytic performance to conventionally synthesized counterparts.

Received 18th August 2020  
Accepted 15th November 2020

DOI: 10.1039/d0ta08107h

rsc.li/materials-a

### Introduction

ZSM-11 zeolite (structural type MEL) was first obtained by Socony Mobil in 1973,<sup>1</sup> which shows a similar pore size and framework density to ZSM-5 zeolite.<sup>2,3</sup> However, unlike ZSM-5 zeolite that has intersecting sinusoidal and straight channels, ZSM-11 zeolite possesses two crossing straight channels (5.3 × 5.4 Å).<sup>2</sup> Thus, the diffusion resistance in the channel of ZSM-11 zeolite is supposed to be weaker than that within ZSM-5 zeolite.<sup>4,5</sup> As a consequence, ZSM-11 exhibits outstanding catalytic performance in the ethene to propene and butene reaction,<sup>6</sup> dehydration of glycerol to acrolein,<sup>4,7</sup> ethanol to propylene reaction,<sup>8</sup> and alkylation of benzene with dimethyl ether/ethanol processes.<sup>9</sup>

Currently, zeolite ZSM-11 is synthesized primarily under hydrothermal conditions, with tetrabutylammonium bromide (TBABr) or tetrabutylammonium hydroxide (TBAOH) as the organic structure-directing agent (OSDA).<sup>7,10</sup> However, unlike ZSM-5 zeolite that could be synthesized without OSDAs,<sup>11–13</sup> the synthesis of ZSM-11 is usually performed under high OSDA content and high temperature. The use of high OSDA content not only increases the cost of production, but also leads to severe environmental pollution. Especially in recent years,

researchers have been devoted to reducing the cost and environmental hazards of zeolite synthesis. Notably, Liang *et al.*<sup>14</sup> proposed a green synthesis process with addition of minimal amounts of water and structure directing agents and shortened steps to prepare nano-sized SSZ-13 zeolite (0.12 μm) using the trans-crystallization strategy. Meanwhile, high crystallization temperature tends to produce the ZSM-5 phase. However, reducing the content of organic templates and crystallization temperature will greatly increase the synthesis time.<sup>15,16</sup> Thus, exploring a simple strategy to accelerate the crystallization of ZSM-11 zeolite under low temperature and organic template concentration is of great interest from both academic and industrial points of view.

Nowadays, several strategies for the rapid synthesis of zeolites have been developed, including the microwave-assisted approach,<sup>17,18</sup> the seeding (including homogeneous and heterogeneous seeds) method<sup>19</sup> and the introduction of crystallization promoters. Among them, the introduction of particular promoters has been widely considered recently. Notably, Yu *et al.*<sup>20</sup> reported that hydroxyl free radicals (·OH) could accelerate the crystallization processes of zeolites. Hu *et al.*<sup>21</sup> found that the incorporation of citric acid (CA) into the synthesis gels of silicoaluminophosphate (SAPO-n) could significantly reduce the crystallization time too. Lately, our group also discovered that *N*-methyl-2-pyrrolidone (NMP) as an organic promoter could increase the crystallization rate of beta zeolite.<sup>22</sup>

Indeed, for the hydrothermal synthesis of ZSM-11 zeolite, the induction period is pretty long, but the growth period is very short.<sup>10</sup> And the induction period accounts for a large part of the

<sup>a</sup>State Key Laboratory of Catalysis, Dalian Institute of Chemical Physics, Chinese Academy of Sciences, Dalian 116023, Liaoning, PR China. E-mail: zhuxx@dicp.ac.cn; slliu@dicp.ac.cn; lyxu@dicp.ac.cn

<sup>b</sup>University of Chinese Academy of Sciences, Beijing 100049, PR China

† Electronic supplementary information (ESI) available. See DOI: 10.1039/d0ta08107h

‡ Equally contributed to this work.

whole synthesis time. So, it is of great significance to shorten the induction period for the fast synthesis of ZSM-11 zeolite. Sandra Burkett and Davis<sup>23,24</sup> investigated the nucleation mechanism of OSDA-mediated synthesis of pure-silica zeolites. They found that the rate of nucleation slowed down when using D<sub>2</sub>O instead of H<sub>2</sub>O during synthesis. It was reported that the hydrogen bonding network of D<sub>2</sub>O is more strong than that of H<sub>2</sub>O, and thus the reconstruction of the network to allow the organic and silicate components to come into contact during nucleation may be slowed in D<sub>2</sub>O. Therefore, we proposed the concept of introducing a strongly polar and aprotic chemical to weaken the hydration layer around TBA<sup>+</sup> and aluminosilicate for rapidly establishing the interaction between them thereby accelerating nucleation.

Herein, we demonstrated a novel approach for rapidly synthesizing ZSM-11 zeolite by adding low-toxic, cost-effective and biodegradable NMP.<sup>25</sup> Meanwhile, the effects of other synthesis parameters on the acceleration effect of NMP were also investigated in depth. In our previous work, the NMP-assisted synthesis of beta zeolite needed high OSDA concentration and the added NMP partially underwent ring-opening reaction in a highly alkaline hydrothermal environment to promote the formation of activated TEA<sup>+</sup>.<sup>22</sup> However, in this work, with the aid of NMP, pure ZSM-11 zeolite could even be rapidly synthesized under an ultra-low content of organic templates (TBA<sup>+</sup>/SiO<sub>2</sub> = 0.02). More importantly, no ring-opening product of NMP was detected throughout the hydrothermal synthesis of ZSM-11 zeolite and the acceleration mechanism was much different from that of beta zeolite.<sup>22</sup> Meanwhile, it was also found that the NMP content, crystallization temperature and Si/Al<sub>2</sub> ratio all significantly affected the acceleration effect of NMP. In addition, the as-synthesized ZSM-11 catalyst exhibited similar hydrothermal stability to the conventional ZSM-11 sample and excellent reaction performance in the alkylation of ethanol with benzene.

## Experimental section

### Synthesis of ZSM-11 zeolite

The samples were synthesized according to our previous work.<sup>26</sup> Typically, at room temperature, 0.54 g of aluminium sulfate (Al<sub>2</sub>(SO<sub>4</sub>)<sub>3</sub>·18H<sub>2</sub>O, 99 wt%), 3.22 g of tetrabutylammonium bromide (TBABr, 99 wt%) and 0.58 g of sodium hydroxide (NaOH, 96 wt%) were dissolved in 28.8 mL H<sub>2</sub>O with fast stirring, and 0.00 or 7.51 g of *N*-methyl-2-pyrrolidone (NMP, 99 wt%) and 9.83 g of silica sol (30 wt%) were added sequentially. The final gel with a molar composition of 1.0 SiO<sub>2</sub>/0.15 Na<sub>2</sub>O/0.016 Al<sub>2</sub>O<sub>3</sub>/0.2 TBABr/40 H<sub>2</sub>O/*x* NMP (*x* = 0.0, 0.5, 1.0, 2.0, 2.5 and 3.0) was introduced into a 75 mL Teflon-lined stainless-steel autoclave rotated at 40 rpm, and crystallized under autogenous pressure at 130 °C. After crystallization, the solid product was separated, washed and dried overnight at 120 °C. All zeolite samples were named Z11-*x*NMP-*y* h, where *x* was the NMP/SiO<sub>2</sub> ratio and *y* was the crystallization time. In addition, the synthesis process of ZSM-11 zeolite with *N*-ethyl-2-pyrrolidone (NEP, 99 wt%) as the promoter was the same as that of NMP.

The synthesized zeolite samples were calcined at 550 °C for 6 h to remove the organic species, and the Na<sup>+</sup>-ZSM-11 zeolites were ion-exchanged three times with 0.8 mol L<sup>-1</sup> NH<sub>4</sub>NO<sub>3</sub> solution (80 °C, 2 h), washed, and dried. The NH<sub>4</sub>-form zeolites were calcined at 530 °C for 4 h to transform into the H-forms, and the corresponding H-form samples were denoted as HZ11-*x*NMP-*y* h.

### Synthesis of ZSM-5 zeolite

Typically, at room temperature, 0.94 g of aluminium sulfate, 6.78 g of tetrapropylammonium hydroxide (TPAOH, 25 wt%) and 0.69 g of sodium hydroxide were dissolved in 6.70 mL H<sub>2</sub>O with fast stirring, and 0.00 or 12.49 g of NMP and 9.83 g of chromatography silica gel (100 wt%) were added sequentially. The final gel with a molar composition of 1.0 SiO<sub>2</sub>/0.10 Na<sub>2</sub>O/0.01667 Al<sub>2</sub>O<sub>3</sub>/0.1 TBABr/8 H<sub>2</sub>O/*x* NMP (*x* = 0.0 and 1.5) was introduced into a 75 mL Teflon-lined stainless-steel autoclave rotated at 60 rpm, and crystallized under autogenous pressure at 120 °C. After crystallization, the solid product was separated, washed and dried overnight at 120 °C.

### Synthesis of MOR zeolite

Typically, at room temperature, 0.36 g of aluminium sulfate, 0.70 g of tetraethylammonium bromide (TEABr, 98 wt%) and 0.58 g of sodium hydroxide were dissolved in 21.85 mL H<sub>2</sub>O with fast stirring, and 0.00 or 7.51 g of NMP and 9.84 g of silica sol (30 wt%) were added sequentially. The final gel with a molar composition of 1.0 SiO<sub>2</sub>/0.196 Na<sub>2</sub>O/0.035 Al<sub>2</sub>O<sub>3</sub>/0.065 TEABr/32 H<sub>2</sub>O/*x* NMP (*x* = 0.0 and 1.5) was introduced into a 75 mL Teflon-lined stainless-steel autoclave rotated at 40 rpm, and crystallized under autogenous pressure at 150 °C. After crystallization, the solid product was separated, washed and dried overnight at 120 °C.

### Characterization

X-ray diffraction (XRD) data used for the phase identification were collected on a PANalytical B. V. X-ray diffractometer using Cu K $\alpha$  radiation ( $\lambda$  = 1.54059 Å), operating at 40 kV and 40 mA, in the range of  $2\theta$  from 5° to 50°. The relative crystallinity (RC) was calculated according to the ratio of the integrated height of the peaks ( $2\theta$  = 7.9° ± 0.1°, 8.8° ± 0.1°, 23.0° ± 0.1°, 23.8° ± 0.1° and 45.0° ± 0.1°) of the sample and the well crystallized sample. X-ray fluorescence (XRF) experiments were performed using a PANalytical zetium X-ray fluorescence spectrometer.

N<sub>2</sub> adsorption and desorption experiments were performed at -196 °C on a Micromeritics ASAP-2020 analyzer. Each sample was degassed at 350 °C for 5 h under a vacuum of 10<sup>-3</sup> Pa before analysis. Fourier transform infrared (FT-IR) spectroscopy was performed using a VERTEX 70 FT-IR spectrometer (Bruker Company). Thermogravimetric analysis (TGA) was performed on a Pyris diamond TG/DTA analyser in air flow (60 mL min<sup>-1</sup>) and a ramp rate of 10 °C min<sup>-1</sup>.

The scanning electron microscopy (SEM) observation was carried out on a HITACHI SU1510 microscope. Transmission electron microscopy (TEM) and selected area electron diffraction (SED) were performed using a JEM-2100 transmission

electron microscope (JEOL Company). The acidic properties of the H-form ZSM-11 zeolites were analyzed using temperature-programmed desorption of ammonia (NH<sub>3</sub>-TPD). The <sup>13</sup>C MAS NMR spectra were recorded on a Bruker AV-400 spectrometer.

### Crystallization kinetics

The crystallization curve of crystallinity with crystallization time at different temperatures was measured and drawn here. The corresponding crystallization time is the crystal nucleation induction period  $t_0$  when the crystallinity is 5%. The reciprocal  $1/t_0$  is used as the nucleation rate  $V_n$ . The slope of the rapidly rising segment of the crystallization curve is the growth rate  $V_g$ . The apparent growth activation energy  $E_g$  and apparent nucleation activation energy  $E_n$  follow the Arrhenius equation:

$$\ln V = \ln C - \frac{E_a}{R} \frac{1}{T}$$

where  $V$  represents the nucleation rate or growth rate,  $E_a$  represents  $E_g$  or  $E_n$ ,  $C$  is a constant,  $R$  is the gas constant (8.314 J mol<sup>-1</sup> K<sup>-1</sup>), and  $T$  is the crystallization temperature.

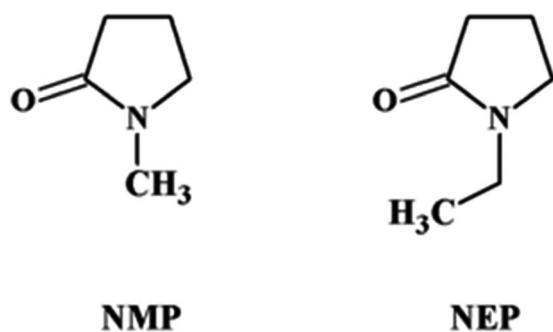
### Catalytic tests

The alkylation of ethanol with benzene was performed in a stainless fixed bed reactor with 0.5 g catalyst. First, the catalyst was pretreated in N<sub>2</sub> (40 mL min<sup>-1</sup>) at 400 °C for 2 h. The reaction was performed under the conditions of 1.5 MPa, 380 or 400 °C, and benzene/ethanol molar ratio of 6.0, and the weight hourly space rate (WHSV) of ethanol was 1 h<sup>-1</sup>. Liquid phase products were analyzed using an Agilent 7890A GC equipped with a PONA capillary column (50 m × 0.2 mm × 0.5 μm) and a FID.

## Results and discussion

### (I) The acceleration effect of NMP

To investigate the effect of the cost-effective and low-toxic lactam NMP (Scheme 1) on ZSM-11 zeolite crystallization, the samples with initial gel compositions of 1.0 SiO<sub>2</sub>/0.016 Al<sub>2</sub>O<sub>3</sub>/0.15 Na<sub>2</sub>O/0.2 TBABr/40 H<sub>2</sub>O/ $x$  NMP ( $x = 0.0$  and 1.5) were hydrothermally treated at 130 °C for 72 h. In the synthesis system containing NMP, the XRD pattern and SEM image of the as-synthesized product Z11-1.5NMP-72 h are shown in Fig. 1A



Scheme 1 Chemical structural formula of NMP and NEP.

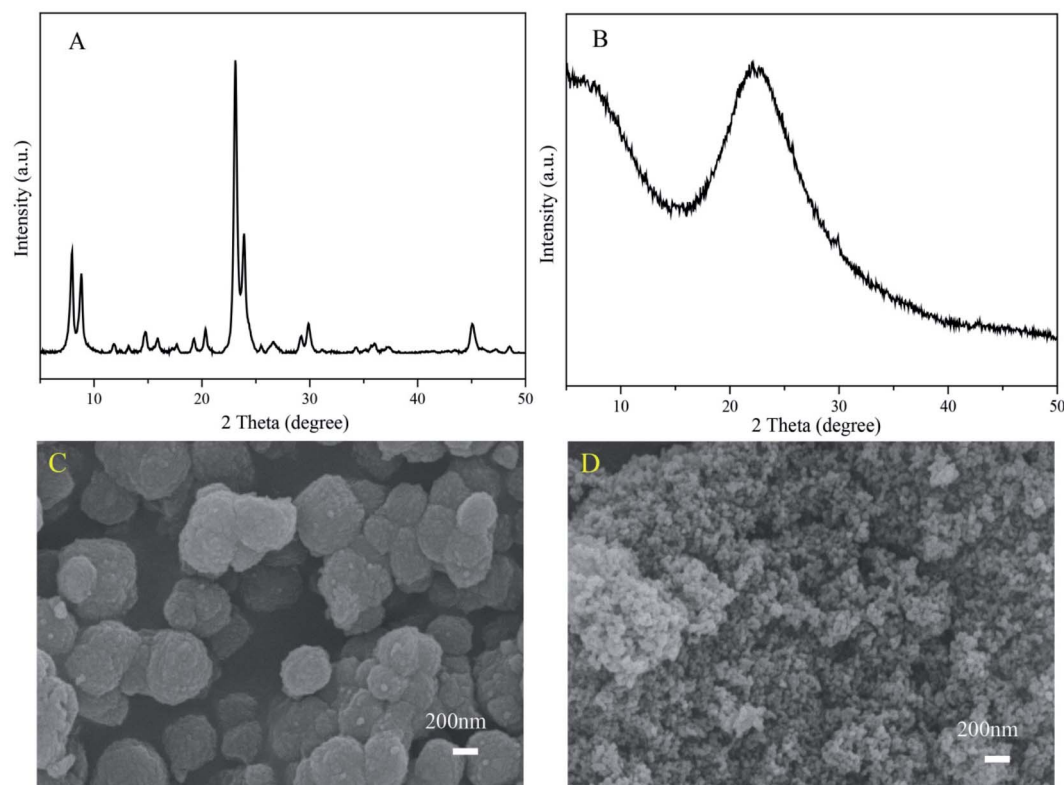


Fig. 1 XRD patterns of Z11-1.5NMP-72 h (A) and Z11-0NMP-72 h (B), SEM images of Z11-1.5NMP-72 h (C) and Z11-0NMP-72 h (D).

and C, respectively. The diffraction peaks with strong intensity accorded with the typical topological characteristics of the MEL framework,<sup>3</sup> while, in the NMP-free synthesis system, the product was still amorphous nanoparticles, as shown in Fig. 1B and D. This indicated that the ZSM-11 zeolite with high crystallinity was rapidly synthesized by employing NMP as a promoter and the crystallization rate of ZSM-11 zeolite was truly increased by NMP.

Furthermore, we tracked the crystallization process of ZSM-11 zeolite to further investigate the acceleration effect of NMP. In the absence of NMP, as confirmed by XRD (Fig. S1B<sup>†</sup>), weak diffraction peaks assigned to poorly crystalline ZSM-11 zeolite emerged at 116 h. Highly crystalline zeolite ZSM-11 was developed until 123 h, while in the presence of NMP, primary ZSM-11 crystals were already visible at 54 h as shown in SEM images (Fig. S3<sup>†</sup>), and the XRD patterns (Fig. S1A<sup>†</sup>) showed that highly crystalline ZSM-11 zeolite was obtained at 68 h. In comparison with the NMP-free synthesis system, the induction period in the presence of NMP was obviously much shorter, while the growth period was similar, as confirmed by the corresponding crystallization curves (Fig. 2). This indicated that NMP plays a crucial role in promoting the nucleation process of ZSM-11 zeolite. In addition, the synthesis system with only NMP as the sole organic additive was also investigated (Fig. S6<sup>†</sup>), and the product was still amorphous even after hydrothermal treatment at 130 °C for 130 h. This indicated that NMP itself cannot direct the crystallization of ZSM-11, but acts as a promoter in the presence of TBA<sup>+</sup>.

## (II) Effects of synthetic parameters on the acceleration effect of NMP

To investigate the effects of synthetic parameters on the acceleration effect of NMP, first, the synthesis was performed under different NMP contents (NMP/SiO<sub>2</sub> = 0.0, 0.5, 1.0, 1.5, 2.0, 2.5 and 3.0) at 130 °C for 68 h. As shown in Fig. S4,<sup>†</sup> the product was amorphous in the absence of NMP. Weak peaks assigned to

poorly crystalline ZSM-11 zeolite appeared when the NMP/SiO<sub>2</sub> was increased to 0.5. Furthermore, the relative crystallinity of the products increased gradually with the increase of NMP/SiO<sub>2</sub> ratio from 0.5 to 3.0. This indicated that the crystallization rate increased with the amount of NMP in the gel.

Meanwhile, the effect of Si/Al<sub>2</sub> ratio on the acceleration effect of NMP was also investigated with the initial gel molar composition of 1.0 SiO<sub>2</sub>/y Al<sub>2</sub>O<sub>3</sub>/0.15 Na<sub>2</sub>O/0.2 TBABr/40 H<sub>2</sub>O/x NMP ( $x = 0.0$  and 1.5;  $y = 0.025, 0.016, 0.0025$  and 0.0004) at 130 °C. As shown in Fig. 3 and S5,<sup>†</sup> the required crystallization time decreased with the increase of Si/Al<sub>2</sub> molar ratio for both synthesis systems with and without NMP. This indicated that the higher the Si/Al<sub>2</sub> molar ratio was, the faster the crystallization rate was. A similar phenomenon had also been reported in the synthesis of ZSM-5 and SSZ-13 zeolite by Toru Wakihara *et al.*<sup>27,28</sup> They thought that aluminosilicate species were more stable than silicate species and were not easily converted into crystals, resulting in a long crystallization period. However, under the same Si/Al<sub>2</sub> ratio, the required crystallization time of ZSM-11 zeolite with NMP was shorter than that without NMP. In fact, with the aid of NMP, the required crystallization time was reduced from 204, 123, 58 and 46 h to 98, 72, 48 and 42 h for the Si/Al<sub>2</sub> molar ratios of 40, 60, 400 and 2500 of the gel, respectively. Especially, the crystallization curves with and without NMP were almost identical for the synthesis system with a Si/Al<sub>2</sub> ratio of 2500. We defined the promote factor (PF) as the ratio of crystallization time needed without promoter and with promoter, which is used to reflect the acceleration ability of a promoter. Interestingly, with the increase of Si/Al<sub>2</sub> molar ratio from 40 to 2500, the PF decreased from 2.08 to 1.10. The results suggested that the acceleration effect of NMP decreased with the increase of Si/Al<sub>2</sub> molar ratio.

In order to obtain ZSM-11 zeolite more economically, we also studied the effect of OSDA concentration on ZSM-11 zeolite synthesis in the presence of NMP. The initial gel with molar compositions of 1.0 SiO<sub>2</sub>/0.0166 Al<sub>2</sub>O<sub>3</sub>/0.15 Na<sub>2</sub>O/*m* TBABr/40 H<sub>2</sub>O/1.5 NMP ( $m = 0.2, 0.1, 0.02$  and 0.01) was hydrothermally treated at 130 °C for 72 h. As shown in Fig. S6 and S7,<sup>†</sup> pure and

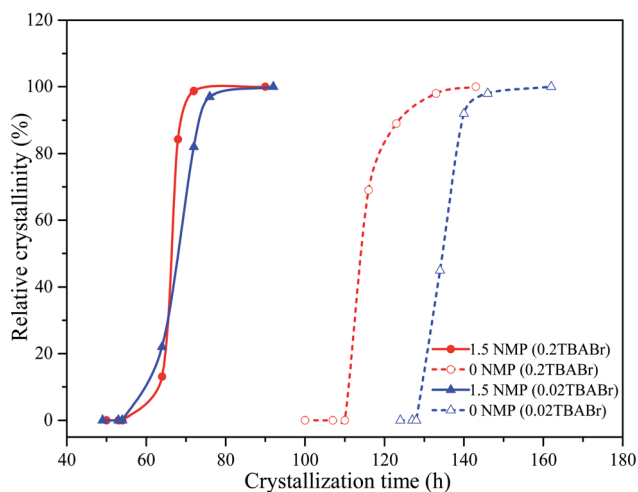


Fig. 2 Crystallization curves of ZSM-11 zeolite synthesized with NMP and without NMP under TBABr/SiO<sub>2</sub> = 0.2 and 0.02 at 130 °C.

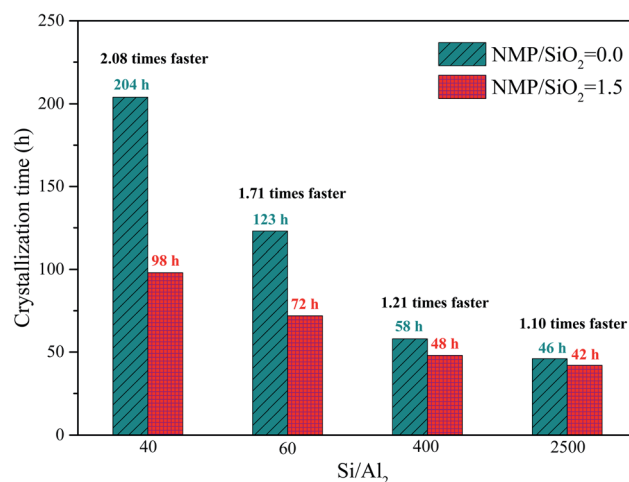


Fig. 3 Si/Al<sub>2</sub> dependence of acceleration effect of NMP at 130 °C.

highly crystalline ZSM-11 zeolite was observed under the condition of  $\text{TBABr}/\text{SiO}_2 = 0.02\text{--}0.2$ . However, when the  $\text{TBABr}/\text{SiO}_2$  ratio was further reduced to 0.01, the product was ZSM-5/ZSM-11 co-crystalline zeolite.

Furthermore, under the ultra-low content of OSDAs ( $\text{TBA}^+/\text{SiO}_2 = 0.02$ ), the crystallization curves of ZSM-11 zeolite are shown in Fig. 2. In the synthesis system without NMP, the nucleation period in the case of  $\text{TPABr}/\text{SiO}_2 = 0.02$  was obviously prolonged in comparison with the case of  $\text{TPABr}/\text{SiO}_2 = 0.2$ . However, in the presence of NMP, ZSM-11 zeolite could still be synthesized rapidly when the  $\text{TPABr}/\text{SiO}_2$  ratio was reduced to 0.02 and the crystallization curve was roughly coincident with a  $\text{TBABr}/\text{SiO}_2$  ratio of 0.2. With the decrease of  $\text{TBABr}/\text{SiO}_2$  ratio from 0.2 to 0.02, the PF increased from 1.71 to 1.84. The above results suggested that the NMP exhibited a more significant acceleration effect under the lower OSDA concentration. It should be noted that NMP is much more low-toxic and cost-effective compared with TBABr. More importantly, the added NMP did not decompose throughout the hydrothermal synthesis (see below). Meanwhile, NMP remained in the mother liquor and was not detected in the solid product (Fig. 5D). This indicated that NMP may act as a recyclable promoter. Thus, this low-OSDA rapid synthesis approach of ZSM-11 zeolite can significantly reduce production costs and is highly efficient and environment-friendly.

Furthermore, we compared the production cost of the NMP-assisted rapid synthesis process with that of the conventional synthesis process. The costs of raw materials, electricity, and labor are shown in Table S1.† Herein, we calculated the theoretical production cost of 500 kg ZSM-11 zeolite as shown in Table S2.† Under the synthesis parameters of  $\text{TBABr}/\text{SiO}_2 = 0.2$  and 0.02, the production costs of the NMP-assisted rapid synthesis process were lower than those of the traditional synthesis process, 91 254 ¥ per ton vs. 94 532 ¥ per ton and 64 134 ¥ per ton vs. 75 012 ¥ per ton, respectively.

If the synthetic mother liquor is recycled, the cost of NMP can be ignored, since NMP does not decompose throughout the hydrothermal synthesis and maintains its intrinsic properties in the mother liquor. Moreover, the  $\text{TBA}^+$  consumption of the two methods are the same ( $\text{TBA}^+/\text{SiO}_2 \approx 0.02$ ) based on the thermogravimetry results (Fig. S16†). Thus, the theoretical production costs for the NMP-assisted rapid synthesis process and traditional synthesis process are 47 012 ¥ per ton and 75 012 ¥ per ton. In a word, the production cost of the NMP-assisted rapid synthesis process is significantly lower than that of the traditional synthesis process.

The acceleration effect of NMP on the synthesis of ZSM-11 zeolite was also investigated at different temperatures with the initial gel molar compositions of  $1.0 \text{ SiO}_2/0.0166 \text{ Al}_2\text{O}_3/0.15 \text{ Na}_2\text{O}/0.2 \text{ TBABr}/40 \text{ H}_2\text{O}/x \text{ NMP}$  ( $x = 0.0$  and  $1.5$ ). As can be seen from Fig. S8 and S9,† the required crystallization time for fully crystalline ZSM-11 decreased with the increase of temperature, due to the temperature effect.<sup>27</sup> At 150, 140 and 130 °C, the PFs were 1.44, 1.56 and 1.71, respectively. The above results showed that the promotion effect of NMP increased with the decrease of crystallization temperature and NMP was an excellent low-temperature crystallization promoter.

In addition, we used TBAOH instead of TBABr as OSDAs, and studied the effect of NMP on the synthesis of ZSM-11 zeolites with molar compositions of  $1.0 \text{ SiO}_2/0.0166 \text{ Al}_2\text{O}_3/0.15 \text{ Na}_2\text{O}/0.2 \text{ TBAOH}/40 \text{ H}_2\text{O}/x \text{ NMP}$  ( $x = 0.0$  and  $1.5$ ) at 130 °C. As shown in Fig. S11 and S12,† in comparison with the case of TBABr as OSDAs (Fig. 2 and 3), the full crystallinity time of ZSM-11 zeolite was obviously longer. Similarly, adding NMP into the synthesis system could also accelerate the nucleation. Furthermore, the PF was 2.70 and the acceleration effect was more obvious. Interestingly, in the case of TBABr as OSDAs, their primary particle size was similar (Fig. S13†) and the granular aggregates of ZSM-11 zeolite obtained by adding NMP were larger than those in the absence of NMP (Fig. S2† (72 h) vs. Fig. S3† (123 h)). However, in the case of TBAOH as OSDAs, the final granular aggregates of ZSM-11 zeolite had a similar size no matter that NMP was added or not (Fig. S14†). The results showed that NMP could not only promote nucleation, but also promote particle aggregation in the presence of bromine ions.

In a word, the NMP content, OSDA content,  $\text{Si}/\text{Al}_2$  ratio, synthesis temperature, and type of OSDAs collectively affect the acceleration effect of NMP. Among them, NMP exhibited a more significant acceleration effect under low  $\text{Si}/\text{Al}_2$  ratios, low OSDA content and low synthesis temperature.

### (III) Investigation of the acceleration mechanism

To unveil the hydrothermal evolution process of ZSM-11 zeolite assisted by NMP, the crystallization processes of ZSM-11 zeolites with molar compositions of  $1.0 \text{ SiO}_2/0.016 \text{ Al}_2\text{O}_3/0.15 \text{ Na}_2\text{O}/0.2 \text{ TBABr}/40 \text{ H}_2\text{O}/x \text{ NMP}$  ( $x = 0.0$  and  $1.50$ ) at 130 °C were investigated in detail. The evolution processes of structural subunits recorded by FT-IR spectroscopy are shown in Fig. 4. For the synthesis system with NMP, only three FT-IR bands centered at  $470 \text{ cm}^{-1}$ ,  $800 \text{ cm}^{-1}$  and  $1113 \text{ cm}^{-1}$  were observed in the samples synthesized at 130 °C for 0 and 50 h, belonging to the bending vibration, symmetric stretching vibration and antisymmetric stretching vibration absorption peak of the T–O–T bond of the gel, respectively.<sup>29</sup> At 64 h, bands at  $1300\text{--}1500 \text{ cm}^{-1}$  assigned to  $\text{TBA}^+$  were observed and the band at  $1113 \text{ cm}^{-1}$  began to split into two bands at  $1222$  and  $1098 \text{ cm}^{-1}$ , which belong to the antisymmetric stretching vibration absorption peaks of the external  $\text{TO}_4$  tetrahedron and internal  $\text{TO}_4$  tetrahedron, respectively.<sup>29</sup> Meanwhile, a weak absorption peak appeared at  $545 \text{ cm}^{-1}$ , which belongs to the double five-membered rings (D5Rs) of crystalline ZSM-11. This indicated that aluminosilicates were combined with  $\text{TBA}^+$  and the ZSM-11 phase began to appear in the product. With the prolongation of crystallization time from 64 to 90 h, the band at  $545 \text{ cm}^{-1}$  of the product became sharper and narrower gradually, and correspondingly, the crystallinity of the product increased. This was consistent with the results of SEM and XRD. Notably, the band of NMP molecules was not observed throughout the crystallization process.

In contrast, in the absence of NMP, the bands assigned to D5Rs and  $\text{TBA}^+$  were observed until 116 h, suggesting that the introduction of NMP could prominently promote incorporation of aluminosilicates with  $\text{TBA}^+$ , polymerization of

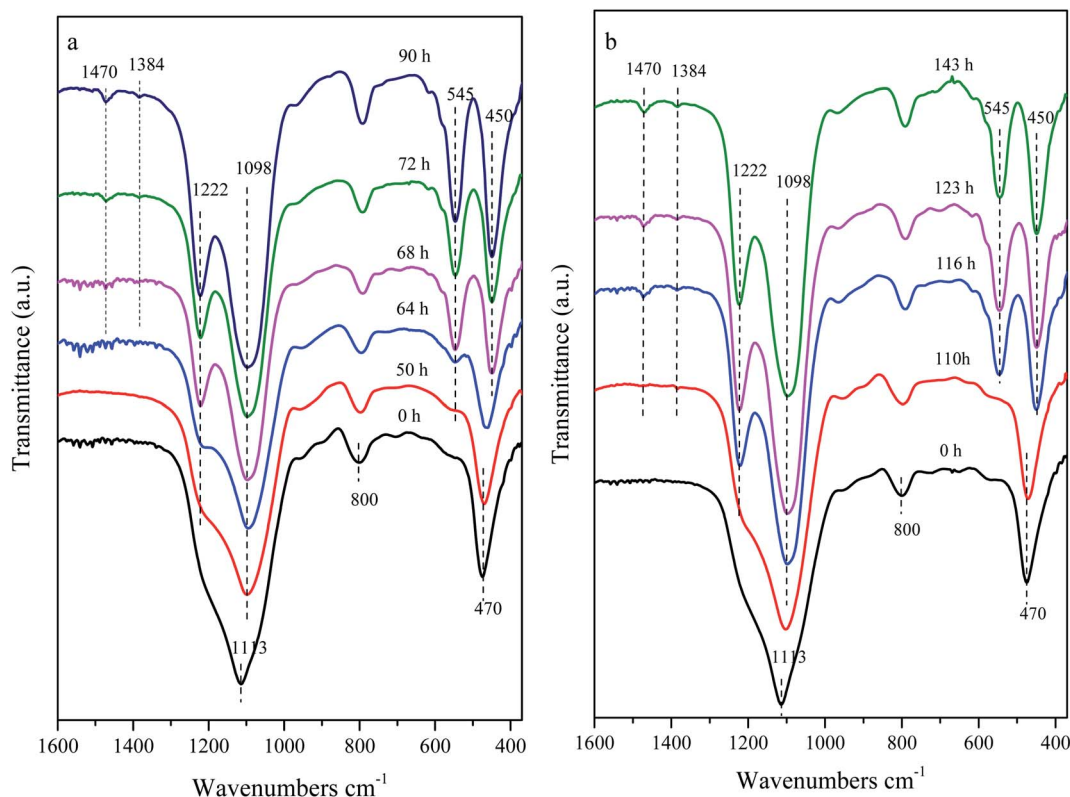


Fig. 4 FT-IR spectra of samples crystallized with ((a)  $\text{NMP}/\text{SiO}_2 = 1.5$ ) and without ((b)  $\text{NMP}/\text{SiO}_2 = 0.0$ ) NMP for different periods of time at  $130^\circ\text{C}$ .

aluminosilicates and the formation of the D5Rs secondary structure units of ZSM-11 zeolite.

The thermal analysis results are shown in Fig. S16.† All samples showed weak weight loss peaks before  $150^\circ\text{C}$ , which corresponded to the removal of adsorbed water in the samples. The weight loss at  $340\text{--}455^\circ\text{C}$  and  $455\text{--}670^\circ\text{C}$  was related to the oxidation and decomposition of  $\text{TBA}^+$  occluded in ZSM-11 zeolite. The synthesis system with (Fig. S16a and b†) and without (Fig. S16c and d†) NMP showed a similar variation tendency, *i.e.*, the quantity of the occluded  $\text{TBA}^+$  species first increased with crystallization time, and then kept almost constant when the crystallization was complete. The weight losses assigned to  $\text{TBA}^+$  of well crystalline products were similar, about 11.5–12.3%. However, the combination rate of  $\text{TBA}^+$  with aluminosilicates in the NMP-containing system was notably faster than that in the NMP-free system. Since NMP was not detectable in the solid product, it may be assumed that the NMP molecules promoted the combination of organic  $\text{TBA}^+$  with inorganic aluminosilicates to form organic–inorganic composite species (key precursor for nucleation), and thus the nucleation process was promoted.

The liquid-state  $^{13}\text{C}$  NMR spectra of the supernatant are shown in Fig. 5. In the absence of NMP, the spectra only exhibited peaks associated with aqueous  $\text{TBA}^+$  (Fig. 5A, marked as a, b, c and d). In the presence of NMP, differently from NMP-mediated rapid synthesis of beta zeolite, in which partial NMP underwent ring-opening and a large amount of TEAOH

decomposed to TEA during hydrothermal treatment,<sup>22</sup> in this work, only peaks associated with aqueous  $\text{TBA}^+$  and NMP (marked as 1, 2, 3, 4 and 5) species were detected in the supernatant. Namely, NMP was relatively stable in our synthesis system and no ring-opening reaction of NMP occurred. This is probably due to the lower alkalinity and crystallization temperature of the synthesis system of ZSM-11 than that of beta zeolite.<sup>22</sup> These results suggest that the NMP-mediated rapid synthesis of ZSM-11 zeolite was much different from that reported on beta zeolite.<sup>22</sup>

Solid-state  $^{13}\text{C}$  NMR spectra (Fig. 5D) revealed that only organic  $\text{TBA}^+$  species existed in the washed products (as also suggested by the IR spectra, see Fig. 4A), implying that only  $\text{TBA}^+$  species were indeed occluded in ZSM-11 zeolite and the added NMP only remained in the mother liquor and kept intact.

The evolution of inorganic elemental compositions of solid products with crystallization time was surveyed by XRF and is summarized in Table S3.† The  $\text{Si}/\text{Al}_2$  ratio of the amorphous product at 0 h was about 46, which was lower than feeding. This indicated that at first more silicon dissolved into the liquid. For the synthesis system with NMP and without NMP, with the prolongation of crystallization time, the ratios of  $\text{Si}/\text{Al}_2$  all increased gradually at first, and then remained basically unchanged. The  $\text{Si}/\text{Al}_2$  ratios of the final product synthesized by adding NMP were slightly higher than that of without NMP (52.1 *vs.* 49.2). Accordingly, the yield of products in the NMP-added system was slightly higher than that of non-NMP-added

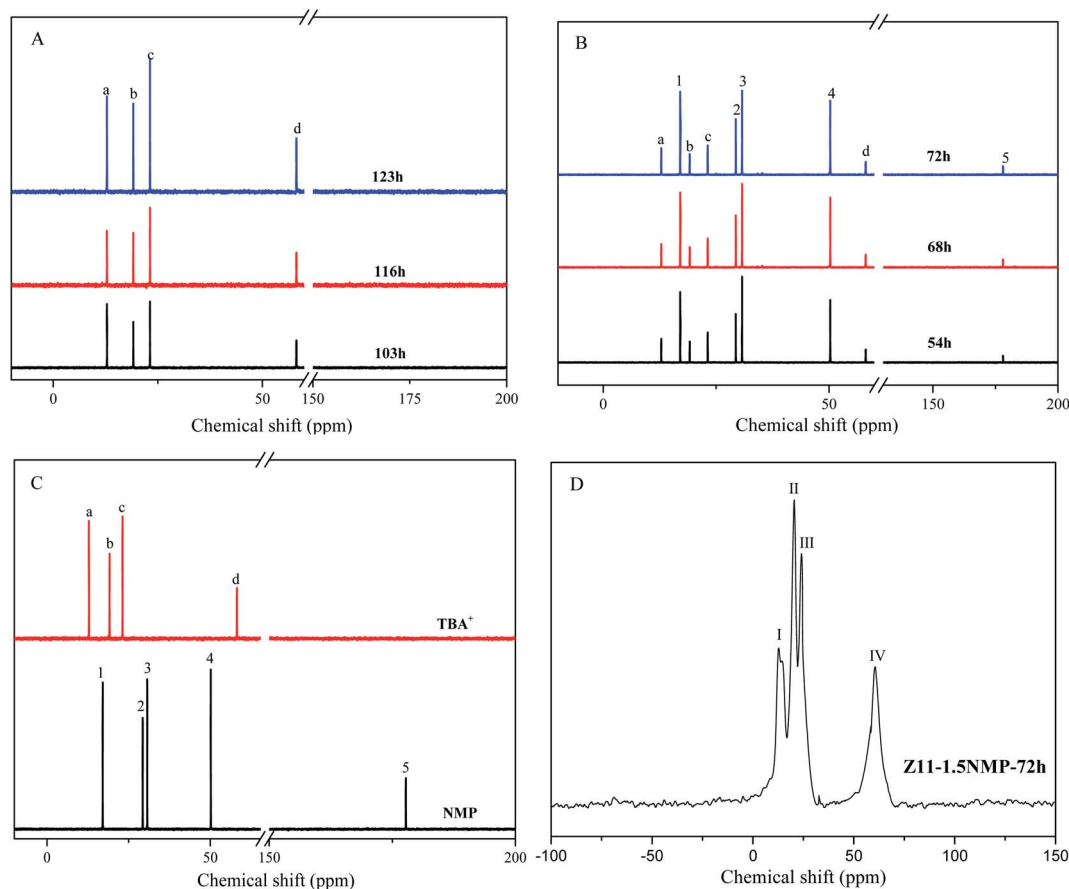


Fig. 5 (A)  $^{13}\text{C}$  liquid NMR spectra of the supernatants synthesized without NMP at various crystallization times; (B)  $^{13}\text{C}$  liquid NMR spectra of the supernatants synthesized with NMP at various crystallization times; (C)  $^{13}\text{C}$  liquid NMR spectra of  $\text{TBA}^+$  and NMP; (D) solid-state  $^{13}\text{C}$  NMR spectra of the solid product synthesized with NMP.

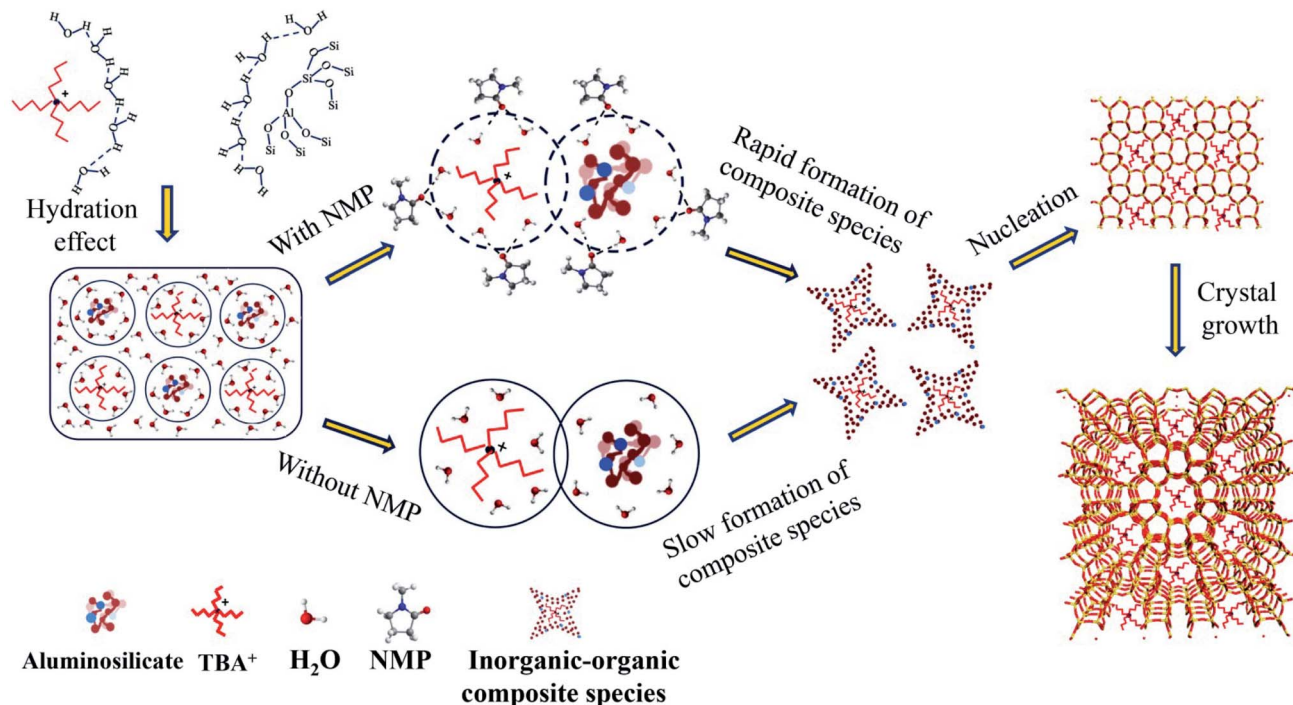
(87 wt% vs. 82 wt%). In addition, we also investigated the  $\text{Si}/\text{Al}_2$  ratio of ZSM-11 zeolite synthesized under the initial gel with different  $\text{Si}/\text{Al}_2$  ratios. The results are shown in Table S4,<sup>†</sup> and the  $\text{Si}/\text{Al}_2$  ratios of the final products synthesized by adding NMP all are higher than that of without NMP too. This may be attributable to the decrease of saturated solubility of water due to the addition of NMP.

Fig. S17<sup>†</sup> displays TEM-EDS results of samples synthesized with NMP and without NMP during the hydrothermal synthesis. During the hydrothermal crystallization process of ZSM-11 zeolite, whether NMP was added or not, the silicon and aluminum species formed a primary amorphous aluminosilicate species with a certain proportion, and silicon and aluminum species were incorporated into the zeolite framework synchronously. This is different from NMP-assisted conversion of USY into hollow beta zeolite, in which the beta crystal with a high  $\text{Si}/\text{Al}_2$  molar ratio was firstly formed.<sup>30</sup> This may be an important reason why NMP assisted synthesis of ZSM-11 zeolite can't form a hollow structure like beta zeolite.<sup>30,31</sup>

The above-described analyses provide valuable insights into the accelerated formation mechanism of ZSM-11 zeolite by the assistance of NMP. Burkett and Davis<sup>23,24</sup> investigated the nucleation mechanism of pure-silicon zeolites with a structure directing agent, and we speculate that ZSM-11 zeolite synthesis

follows a similar nucleation mechanism. As shown in Scheme 2, first, ordered hydration spheres around the  $\text{TBA}^+$  cation and soluble aluminosilicate species formed due to the hydration effect, and then they collided which led to overlapping of hydration spheres. The water molecules surrounding the OSDAs were replaced by aluminosilicate species as the key step in the nucleation process. Subsequently, favorable electrostatic and van der Waals contacts between the alkyl chains of  $\text{TBA}^+$  and the aluminosilicate species were established and generated the inorganic-organic composite species. These species provide the means by which the geometry of the OSDAs was translated into the zeolite pore architecture.

According to the experimental results (Fig. 2), NMP mainly played the role of accelerating the nucleation. Burkett and Davis<sup>23,24</sup> found that the rate of nucleation slowed down when using  $\text{D}_2\text{O}$  instead of  $\text{H}_2\text{O}$ , due to the stronger hydrogen bonding network of  $\text{D}_2\text{O}$  than that of  $\text{H}_2\text{O}$ . Namely, strong hydrogen bonding networks hamper the reconstruction of the networks to allow the organic and silicate components to come into contact during nucleation. NMP is a strongly polar and aprotic lactam.<sup>25</sup> As an ideal strong hydrogen-bond-acceptor (HBA) solvent, NMP can interact with water molecules through hydrogen bonding. Molecular dynamic simulation results showed that NMP has a strong structural effect on water



Scheme 2 Proposed mechanism of the NMP-assisted rapid synthesis of ZSM-11 zeolite.

molecules around it.<sup>32,33</sup> And thermodynamic analysis of NMP–H<sub>2</sub>O mixtures showed that the three-dimensional network of hydrogen bonds in H<sub>2</sub>O underwent transformations and was broken with the addition of NMP.<sup>34</sup> Thus, we speculated on the accelerating nucleation mechanism of NMP. As shown in Scheme 2, in the suitable aluminosilicate synthesis system containing NMP, when NMP molecules were close to the TBA<sup>+</sup> and aluminosilicate species, NMP could break the hydration layer around them. Due to the lack of the barrier of the hydration layer, it was more easy and rapid to establish interaction between TBA<sup>+</sup> and aluminosilicate species to generate the inorganic–organic composite species that serve as the key components in nucleation and crystal growth. Thus, NMP could accelerate the nucleation and promote the synthesis of ZSM-11 zeolite. At present, the accelerated nucleation mechanism of NMP lacks direct experimental evidence. In future work, direct experimental evidence to prove the mechanism will be followed up.

In addition, we calculated the apparent nucleation activation energy and apparent growth activation energy of ZSM-11 zeolite synthesized with and without NMP based on the crystallization curves in Fig. S8.† As shown in Fig. S10 and Table S5,† the apparent growth activation energies with and without NMP are similar, 136.4 and 134.1 kJ mol<sup>-1</sup>, respectively. However, the apparent nucleation activation energies with and without NMP are 62.6 and 91.8 kJ mol<sup>-1</sup>, respectively. Clearly, the addition of NMP to the synthesis system could reduce the apparent nucleation activation energy. We speculated that NMP broke the hydration layer around TBA<sup>+</sup> and aluminosilicate, enabling the water molecules around the TBA<sup>+</sup> to be replaced more easily by aluminosilicate to generate the inorganic–organic composite

species, thus reducing the apparent nucleation activation energy as shown in Fig. 6.

The significant variation of the acceleration effect of NMP under different Si/Al<sub>2</sub> ratios may be due to the fact that the hydration of aluminosilicate is enhanced due to the charge density increase with the increase of aluminum species. That is, the hydration layer around aluminosilicate intensifies with the decrease in Si/Al<sub>2</sub> ratio. Breaking the barrier of the hydration layer and establishing the interaction between TBA<sup>+</sup> and aluminosilicate were more difficult, and hence the nucleation process was restricted, while, in the presence of NMP, the hydration layer around TBA<sup>+</sup> and aluminosilicate was weakened, and therefore, the nucleation was greatly accelerated. However, with the increase of Si/Al<sub>2</sub> ratio, the hydration around

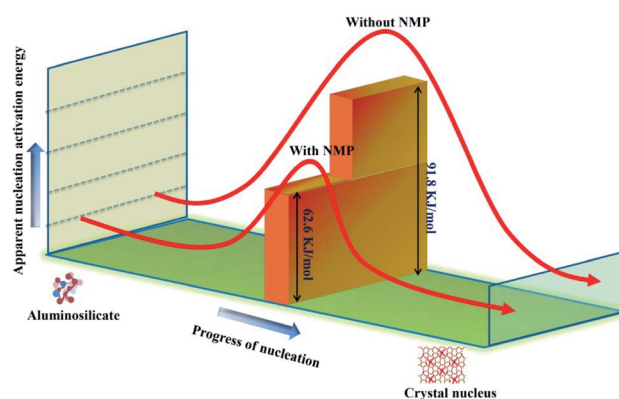


Fig. 6 Diagram of reducing the nucleation activation energy of ZSM-11 zeolite with NMP as the promoter.

aluminosilicate was weakened too. It was easier to establish interaction between  $\text{TBA}^+$  and aluminosilicate. Thus, the nucleation was fast under a high  $\text{Si}/\text{Al}_2$  ratio, and the acceleration effect of NMP was not as obvious as that under a low  $\text{Si}/\text{Al}_2$  ratio.

Furthermore, we used NEP instead of NMP as the promoter to carry out the verification experiment under the same gel composition and crystallization conditions. NEP can also form hydrogen bonds with  $\text{H}_2\text{O}$  molecules, but it is weaker than NMP. Namely, the ability to break the hydrated layer of NEP is weaker than that of NMP. Thus, the crystallization time of the synthesis system with NEP should be shorter than that without promoter, but longer than that with NMP, as demonstrated in Fig. S18.†

Thermodynamic analysis results showed that an increasing NMP concentration led to breakage of a three-dimensional hydrogen bonding network of waters in NMP & water mixtures.<sup>34</sup> Therefore, the higher the NMP content ( $\text{NMP}/\text{SiO}_2 = 0.0\text{--}2.5$ ) in the hydrothermal synthesis system of ZSM-11, the more obvious the acceleration effect. But by adding excessive NMP ( $\text{NMP}/\text{SiO}_2 \geq 2.5$ ), the crystallization rate would not increase due to the dilution effect. Obviously, the increase of crystallization temperature itself would weaken the hydration effect around the template and aluminosilicate in the hydrothermal synthesis system. Thus, when NMP was added to the synthesis system at a higher temperature, the promotion effect of NMP was weakened, and NMP had good low temperature acceleration performance.

Overall, NMP itself does not decompose during the synthesis process, as the promoter, and NMP accelerated the nucleation of ZSM-11 zeolite mainly by promoting the binding of  $\text{TBA}^+$  and aluminosilicate that are surrounded by the hydrated layer. Meanwhile, the NMP content,  $\text{Si}/\text{Al}_2$  ratio, and synthesis temperature all affect the binding rate.

Based on our proposed promotion mechanism, the crystallization of MFI and MOR zeolites was also accelerated successfully by adding NMP to the synthesis systems. As shown in Fig. S19,† in the synthesis systems containing NMP, MFI and MOR zeolites could be obtained by crystallization at  $120^\circ\text{C}$  for 24 h and  $150^\circ\text{C}$  for 94 h respectively. However, in the NMP-free synthesis system, the corresponding products were still amorphous. This result suggested that the present strategy may be generalized for accelerating the crystallization of zeolites synthesized with cationic OSDAs.

#### (IV) Hydrothermal stability and reaction performance

In general, the hydrothermal stability of the zeolite catalyst is a crucial factor affecting its practical application, especially for reactions containing water (such as the alkylation of benzene with ethanol/methanol). Therefore, we compared the hydrothermal stability of ZSM-11 zeolites with a similar  $\text{Si}/\text{Al}_2$  ratio prepared with and without NMP (Table S6†). In general, the change of crystallinity before and after high temperature steam treatment is an index to measure the hydrothermal stability of zeolite. The XRD patterns of HZ11-1.5NMP-72 h and HZ11-0NMP-123 h before and after 100% steam treatment

at  $700^\circ\text{C}$  for 6 h are shown in Fig. 7. The crystal structure of the sample could be well maintained, and the RCs of HZ11-1.5NMP-72 h ( $700^\circ\text{C}$ , 6 h) and HZ11-0NMP-123 h ( $700^\circ\text{C}$ , 6 h) remain at 98% (where the RC of HZ11-1.5NMP-72 h was assumed as 100%) and 97% (where the RC of HZ11-0NMP-123 h was assumed as 100%), respectively, after the steam treatment. According to  $\text{N}_2$  adsorption-desorption measurement results (Table S6†), HZ11-1.5NMP-72 h ( $700^\circ\text{C}$ , 6 h) and HZ11-0NMP-123 h ( $700^\circ\text{C}$ , 6 h) still had an abundant microporous structure although the microporous volume slightly decreased. As shown in Fig. S20,† HZ11-1.5NMP-72 h and HZ11-0NMP-123 h possessed a similar acid amount. And after the steam treatment with  $700^\circ\text{C}$  for 6 h, although the acid amount decreased, they still showed a nearly equal acid amount. The above results demonstrated that the zeolite ZSM-11 synthesized by NMP assistance exhibited similar hydrothermal stability to that synthesized without NMP.

The reaction performance of selected samples was evaluated in gas phase alkylation of ethanol with benzene. Table 1 displays the reaction performances of HZ11-1.5NMP-72 h ( $700^\circ\text{C}$ , 6 h) and HZ11-0NMP-123 h ( $700^\circ\text{C}$ , 6 h). The selectivities of liquefied petroleum gas and dry gas over the two catalysts were very low, and the selectivity of the liquid hydrocarbon products was as high as *ca.* 98% for whole reaction processes. As shown in Table 1, the two samples showed similar reaction activity (conversion of ethanol was 100%). The benzene conversions of the two samples were 14.57% and 15.16% respectively (the highest conversion of benzene was 16.67% in theory). Ethylbenzene and diethylbenzene were the main liquid hydrocarbon products. The selectivities of ethylbenzene were 83.30% and 83.86%, and the values of ethylation products (ethylbenzene and diethylbenzene) were 97.95% and 97.83%, respectively.

The alkylation of ethanol with benzene is a typical reaction catalyzed by acid.<sup>35</sup> HZ11-0NMP-123 h ( $700^\circ\text{C}$ , 6 h) and HZ11-1.5NMP-72 h ( $700^\circ\text{C}$ , 6 h) samples also possessed similar acid amounts (Fig. S20†), besides the superior hydrothermal

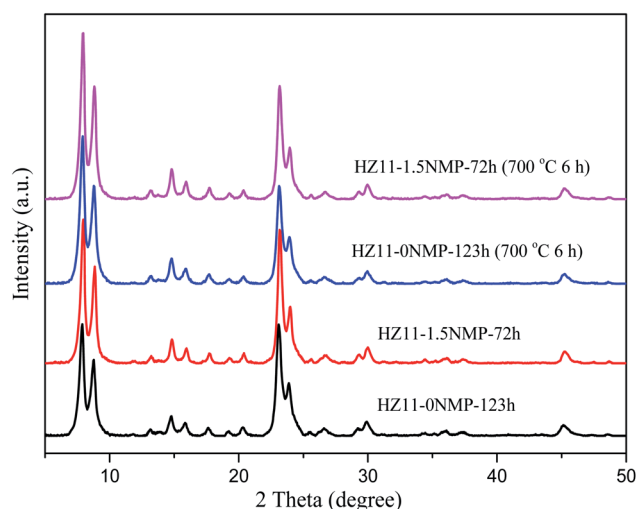


Fig. 7 XRD patterns of samples before and after steaming treatment.

**Table 1** Reaction performance over HZ11-0NMP-123 h (700 °C, 6 h) and HZ11-1.5NMP-72 h (700 °C, 6 h) catalysts for alkylation of ethanol with benzene<sup>a</sup>

Catalyst	Conversion/%		Product selectivity/%						
	Benzene	Ethanol	Ethylbenzene	Ethylation	Methylbenzene	C3 benzene*	Xylene	Non-aromatic hydrocarbon	Others
HZ11-0NMP-123 h (700 °C, 6 h)	14.57	100	83.30	97.95	0.22	0.67	0.04	0.16	0.96
HZ11-1.5NMP-72 h (700 °C, 6 h)	15.16	100	83.86	97.83	0.22	0.72	0.05	0.15	1.03

<sup>a</sup> Reaction conditions:  $m(\text{catalyst}) = 0.5 \text{ g}$ ;  $400 \text{ }^\circ\text{C}$ ;  $1.5 \text{ MPa}$ ;  $\text{WHSV}(\text{ethanol}) = 1.0 \text{ h}^{-1}$ ;  $n(\text{benzene})/n(\text{ethanol}) = 6/1$ ; time-on-stream = 46 h. \*: propylbenzene and ethyltoluene.

stability (Fig. 7). Hence the conversion of reactants and the selectivity of products over the two catalysts were similar. In addition, the HZ11-1.5NMP-72 h catalyst possessed good reaction performance. As shown in Fig. S21,† during the 500 h life test, the conversion of ethanol and benzene remained at 100% and over 15%, respectively. The selectivities of ethylbenzene and ethylation products nearly kept at about 90% and 96%, respectively.

## Conclusions

In summary, we have developed an economical strategy for rapid synthesis of ZSM-11 zeolite by the introduction of NMP as a promoter. The addition of NMP could weaken the hydration interaction between H<sub>2</sub>O and inorganic/organic species (aluminosilicate and TBA<sup>+</sup>). As a result, the combination of aluminosilicate with TBA<sup>+</sup> (key step for nucleation), the formation of the inorganic–organic composite (key precursor for nucleation) and the nucleation process of ZSM-11 zeolite were greatly promoted. The NMP content, Si/Al<sub>2</sub> ratio and synthesis temperature all influenced the acceleration effect of NMP. Especially, NMP significantly promoted the crystallization of ZSM-11 zeolite under a low Si/Al<sub>2</sub> ratio and crystallization temperature. Furthermore, the as-synthesized ZSM-11 catalyst exhibited similar hydrothermal stability to the conventional ZSM-11 sample and excellent reaction performance in the alkylation of ethanol with benzene.

## Conflicts of interest

There are no conflicts of interest to declare.

## Acknowledgements

This work was supported by the National Natural Science Foundation of China (No. 21773233), Dalian Science and Technology Innovation fund project (2019J12GX027), DICP (Grant: DICP ZZBS201806), Liaoning Revitalization Talents Program (XLYC1901006 and XLYC1908010), and CNPC-DICP Joint Research Center, Strategic Priority Research Program of the CAS (XDA21031103).

## Notes and references

- P. Chu and N. J. Woodbury, *US Pat.*, 3709979, 1973.
- G. T. Kokotailo, P. Chu, L. S. Lawton and M. W. Meier, *Nature*, 1978, **275**, 119–120.
- D. M. Bibby, N. B. Milestone and L. P. Aldridge, *Nature*, 1979, **280**, 664–665.
- Y. Gu, N. Cui, Q. Yu, C. Li and Q. Cui, *Appl. Catal., A*, 2012, **429–430**, 9–16.
- L. Zhang, S. Qiao, Y. Jin, L. Cheng, Z. Yan and G. Q. Lu, *Adv. Funct. Mater.*, 2008, **18**, 3834–3842.
- S. Follmann and S. Ernst, *New J. Chem.*, 2016, **40**, 4414–4419.
- J. Ding, L. Wang, Z. Zhang, S. Zhao, J. Zhao, Y. Lu and J. Huang, *ACS Sustainable Chem. Eng.*, 2019, **7**, 16225–16232.
- K. Inoue, K. Okabe, M. Inaba, I. Takahara and K. Murata, *React. Kinet., Mech. Catal.*, 2010, **101**, 227–235.
- H. Liu, S. Xie, W. Xin, S. Liu and L. Xu, *Catal. Sci. Technol.*, 2016, **6**, 1328–1342.
- S. Wei, Y. Xu, C. Che, K. Zhu, Z. Jin and X. Zhu, *React. Kinet., Mech. Catal.*, 2019, **127**, 803–823.
- S. D. Kim, S. H. Noh, J. W. Park and W. J. Kim, *Microporous Mesoporous Mater.*, 2006, **92**, 181–188.
- F. Pan, X. Lu, T. Wang and Y. Yan, *Mater. Lett.*, 2017, **196**, 245–247.
- X. Huang and Z. Wang, *Chin. J. Catal.*, 2011, **32**, 1702–1711.
- J. Liang, Y. Mi, G. Song, H. Peng, Y. Li, R. Yan, W. Liu, Z. Wang, P. Wu and F. Liu, *J. Hazard. Mater.*, 2020, **398**, 122986.
- J. Aguado, D. P. Serrano, J. M. Escola and J. M. Rodríguez, *Microporous Mesoporous Mater.*, 2004, **75**, 41–49.
- X. Guo, Y. Liu, X. Wang, Y. Chen, W. Zhang, X. Han, X. Bao and L. Lin, *J. Dalian Univ. Technol.*, 2001, **41**, 426–430.
- A. R. Majdinasab, P. K. Manna, Y. Wroczynskij, J. van Lierop, N. Cicek, G. K. Tranmer and Q. Yuan, *Mater. Chem. Phys.*, 2019, **221**, 272–287.
- J. F. Azzolina, P. Isabelle, E. Lionel and L. B. Pierella, *Microporous Mesoporous Mater.*, 2014, **198**, 22–28.
- A. Javdani, J. Ahmadpour and F. Yaripour, *Microporous Mesoporous Mater.*, 2019, **284**, 443–458.
- G. Feng, P. Cheng, W. Yan, M. Boronat, X. Li, J. Su, J. Wang, Y. Li, A. Corma, R. Xu and J. Yu, *Science*, 2016, 351.
- X. Liu, T. Wang, C. Wang, H. Shi, P. Zhang, X. Li, Z. Wang, Z. Yao and M. Hu, *Chem. Eng. J.*, 2020, **381**, 122759.

- 22 D. Zhao, W. Chu, Y. Wang, X. Zhu, X. Li, S. Xie, J. An, W. Xin, S. Liu and L. Xu, *J. Mater. Chem. A*, 2018, **6**, 24614–24624.
- 23 S. L. Burkett and M. E. Davis, *Chem. Mater.*, 1995, **7**, 920–928.
- 24 S. L. Burkett and M. E. Davis, *Chem. Mater.*, 1995, **7**, 1453–1463.
- 25 J. Abolghasem, A. A. F. Mohammad and S. Ali, *Int. J. Pharm. Pharm. Sci.*, 2010, **13**, 524–535.
- 26 L. Zhang, H. Liu, X. Li, S. Xie, Y. Wang, W. Xin, S. Liu and L. Xu, *Fuel Process. Technol.*, 2010, **91**, 449–455.
- 27 M. Deguchi, K. Iyoki, C. Anand, Y. Yanaba, T. Yoshikawa, T. Okubo and T. Wakihara, *Microporous Mesoporous Mater.*, 2018, **270**, 200–203.
- 28 Z. Liu, T. Wakihara, K. Oshima, D. Nishioka, Y. Hotta, S. P. Elangovan, Y. Yanaba, T. Yoshikawa, W. Chaikittisilp, T. Matsuo, T. Takewaki and T. Okubo, *Angew. Chem., Int. Ed.*, 2015, **54**, 5683–5687.
- 29 J. C. Jansen, F. J. Gaag and H. Bekkum, *Zeolites*, 1984, **4**, 369–372.
- 30 X. Wang, D. Zhao, W. Chu, C. Yang, Y. Wang, X. Zhu, W. Xin, Z. Liu, H. Wang, S. Liu and L. Xu, *Microporous Mesoporous Mater.*, 2020, **294**, 109944.
- 31 D. Zhao, Y. Wang, W. Chu, X. Wang, X. Zhu, X. Li, S. Xie, H. Wang, S. Liu and L. Xu, *J. Mater. Chem. A*, 2019, **7**, 10795–10804.
- 32 T. J. Carver, M. G. B. Draw and P. Mark Rodger, *Phys. Chem. Chem. Phys.*, 1999, **1**, 1807–1816.
- 33 G. Jia, F. Wang, X. Yang and J. Qian, *J. Mol. Liq.*, 2014, **197**, 328–333.
- 34 A. M. Zaichikov, *Russ. J. Gen. Chem.*, 2006, **76**, 626–633.
- 35 C. Yang, S. Xie, H. Liu, W. Xin, C. Feng, X. Li, S. Liu, L. Xu and P. Zeng, *Catal. Lett.*, 2018, **148**, 2030–2041.